Journal of Geophysical Research: Solid Earth

RESEARCH ARTICLE
10.1029/2018JB016097

Bounding the Moment Deficit Rate on Crustal Faults Using Geodetic Data: Application to Southern California

Jeremy Maurer[1,2], **Kaj Johnson**[3], **and Paul Segall**[1]

[1]Department of Geophysics, Stanford University, Stanford, CA, USA, [2]Now at the Jet Propulsion Laboratory, California Institute of Technology, Pasadena, CA, USA, [3]Department of Earth and Atmospheric Sciences, Indiana University, Bloomington, IN, USA

Key Points:
- We apply a new method, COBE, to estimate the current Moment Deficit Rate (MDR) in Southern California
- MDR for Southern California may be significantly higher than the average seismic moment rate since 1850
- We report MDR for individual fault segments and show that many could host significant earthquakes

Supporting Information:
- Supporting Information S1

Correspondence to:
J. Maurer,
jlmaurer@alumni.stanford.edu

Citation:
Maurer, J., Johnson, K., & Segall, P. (2018). Bounding the moment deficit rate on crustal faults using geodetic data: Application to Southern California. *Journal of Geophysical Research: Solid Earth*, *123*, 11,048–11,061. https://doi.org/10.1029/2018JB016097

Received 12 MAY 2018
Accepted 26 NOV 2018
Accepted article online 29 NOV 2018
Published online 15 DEC 2018

Abstract The interseismic moment deficit rate (MDR) constrains the potential for future moment release in earthquakes. Published estimates of the geodetic MDR in Southern California vary by a factor of 3 depending on the type of forward model, method of estimation, and data quality. It is our aim to determine to what degree these discrepancies may be explained by quantifying the uncertainty for a given class of forward models, accounting for data errors and limited model resolution. We apply a new method, the Constrained Optimization Bounding Estimator, to bound the MDR in Southern California using geodetic data and an elastic plate-block model. Total MDR ranges from 1.3 to 2.0 $\times$ 10^{19} N m/yr, equivalent to one M_W 8.17–8.31 over 160 years, higher than the observed seismic moment since 1850. This observation, together with published estimates of off-fault moment rate, could imply that significant permanent (inelastic) deformation is taking place in Southern California or that future earthquakes will make up the difference. Uncertainty in MDR from Constrained Optimization Bounding Estimator using a single model is comparable to the range of published MDR estimates using elastic block models but about a factor of 8 smaller than the range of all published models. Thus, the choice of forward model dominates the uncertainty in MDR for Southern California. While additional data would be helpful for constraining the MDR, as much or more effort is needed to quantify the prediction errors associated with a given model and to develop observations that narrow the possible range of forward models under consideration.

Plain Language Summary We all know that Southern California is seismically active, but how many large earthquakes are possible in the upcoming decades, and where will they occur? The answer to these questions is obviously critical for preparing for future earthquakes, but to get the answers, we need to know the buildup of moment deficit (a measure of earthquake potential) over time. There are different ways to estimate the moment deficit, but many published estimates do not agree, and it is hard to determine whether the differences are important or arise due to data limitations. That is where we come in. We developed a method to measure the uncertainty due to limited data and compared that to the differences between models. We show that there are big differences between models, but most are consistent with one fact: there is more moment deficit accruing then has been released in the last 160 years. However, we do not know if this means one additional very large earthquake, several moderate-sized events, or strain accommodated through distributed aseismic processes. Improved and more consistent models of the Earth's crust is an important future step needed to accurately answer this question.

1. Introduction

Geodetic data such as Global Navigation Satellite Systems (GNSS) and Interferometric Synthetic Aperture RADAR provide information to constrain surface deformation and strain rates. The most recent version of the Unified California Earthquake Rupture Forecast (UCERF3) incorporated geodetic data into the seismic hazard forecast for California for the first time (Field et al., 2014). When combined with a model of crustal faults, geodetic data can provide information on the interseismic moment deficit rate (MDR) and the slip deficit rate (SDR). The SDR is defined as the difference between the current interseismic rate and the long-term slip rate, which is the fault slip rate averaged over many earthquake cycles. MDR is defined as the integral of the SDR over total fault area

$$\dot{M}_d = G \int_A \dot{s}(\xi) \mathrm{d}A = GA\dot{\bar{s}}, \tag{1}$$

where G is shear modulus, A is fault area, $\dot{s}(\xi)$ is the SDR as a function of position ξ on the fault, and $\bar{\dot{s}}$ is the spatially averaged SDR. (For simplicity we write SDR without additional notation; it should not be confused with the interseismic slip rate, e.g., $\dot{s} \equiv \dot{s}_{\infty} - \dot{s}_{\text{inter}}$.) Moment deficit accumulating over time may be released in large earthquakes; the MDR provides a first-order constraint on earthquake potential. Ideally, MDR should be obtained without the regularization required in traditional SDR models.

In Southern California, there is a large range of MDR estimates from previously published studies, but none have taken all sources of uncertainty into account. Sources of uncertainty include (1) the full variance-covariance of the geodetic observations, (2) imperfect resolution of slip deficit at depth, due to existence of a model null space, and (3) prediction errors resulting from an inaccurate Earth model. Because moment deficit accrued during the interseismic period must be accommodated in some way, as coseismic slip, transient aseismic slip (e.g., afterslip), or distributed deformation, it is vital to understand what bounds on MDR are allowed by the data in order to constrain seismic hazard. All three sources of uncertainty must be accurately quantified to accomplish this, which in general is a difficult problem. In this study, we employ a new method for rigorously quantifying uncertainty due to (1) and (2). In section 4 we briefly consider how future work could address (3).

1.1. Disparities Between Previous Estimates of the MDR in Southern California

The top half of Figure 1 shows the annual MDR estimated by previous studies (colored squares and bars). We also show the total historic seismic moment estimated for Southern California in the interval 1852–2012, computed using the seismicity catalog compiled for UCERF3 (Field et al., 2014, Appendix K). We included all earthquakes with magnitude M_W 4 and greater. Events in the catalog (shown in supporting information Figure S1) are located between 31.5° and 37.5° north latitude and between 114° and 122° west longitude (3,481 total events). The average moment of these events is approximately 1.33×10^{19} N m/yr (total 2.13×10^{21} Nm), equivalent to about one M_W 6.71 per year, shown by the left vertical black dashed line in Figure 1. Obviously, the catalog is incomplete at low magnitudes prior to 1932, and we have not corrected local magnitudes to moment magnitudes; however, events that are M_W 6 and greater contribute more than 95% of the total moment release (about 2×10^{21} Nm total or 1.27×10^{19} N m/yr annually). The right black dashed line in Figure 1 is an estimate of the upper bound on the seismic moment, which would be the case if a M_W 8 event were to occur tomorrow in Southern California, corresponding to an annual MDR of 2.03×10^{19} N m/yr. The shaded region between the two dashed lines represents the uncertainty in the observed moment.

Some early estimates of the geodetic MDR used Kostrov-type summation by computing surface strain rates and converting to MDR by summing and multiplying by seismogenic depth and shear modulus (Savage & Simpson, 1997; Ward, 1994, 1998). These estimates are shown by the blue squares and bar in Figure 1. The Working Group on California Earthquake Probabilities found a geodetically estimated moment deficit accumulation rate of 0.94×10^{19} N m/yr and a geologically estimated rate of 0.93×10^{19} N m/yr. Ward (1994) and Savage and Simpson (1997) obtained MDR estimates of 1×10^{19} (M_W 6.63 per year) and $0.8–0.9 \times 10^{19}$ N m/yr (M_W 6.57–6.6), respectively, from surface velocities estimated using GNSS and Very Long Baseline Interferometry (Feigl et al., 1993). Ward (1998), using more recent GNSS data, estimated a higher annual rate of $1.06–1.40 \times 10^{19}$ N m/yr (M_W 6.65–6.73) for a seismogenic depth of 11 km and $1.22–1.62 \times 10^{19}$ N m/yr (M_W 6.69–6.77) for a seismogenic depth of 12.7 km (blue bar in Figure 1). These early studies approximately matched the historical moment release for their choice of seismogenic depth. Other studies used a variety of methods for estimating MDR. Stein and Hanks (1998) report a range for MDR of $0.8–1.3 \times 10^{19}$ N m/yr, with the lower bound given by assuming a single fault accommodating the total plate rate. Shen-Tu et al. (1999) estimated a relatively high MDR of 1.46×10^{19} or 2×10^{19} N m/yr, using a locking depth of 11 or 15 km, respectively, and the Kostrov method with constraints from Quaternary fault slip rates and plate motions from NUVEL-1A.

UCERF3 included several different MDR estimates (Field et al., 2014). Uncertainties in fault slip rates from geologic studies were used to obtain the equivalent range in MDR shown by the green dashed line in Figure 1. Note that this uncertainty, including only the range possible from geologic slip rate estimates, is larger than one M_W 8 equivalent moment over 160 years. Several kinematic deformation models were also included, constrained by GNSS-derived velocities and geologic fault slip rates. Bird (2009) obtained an estimate of 1.78×10^{19} N m/yr (M_W 6.80) using the code Neokinema, while a buried elastic dislocation model by Zeng and Shen (2014) gave a total moment rate of 2.11×10^{19} N m/yr (M_W 6.85). These models are shown in red in Figure 1.

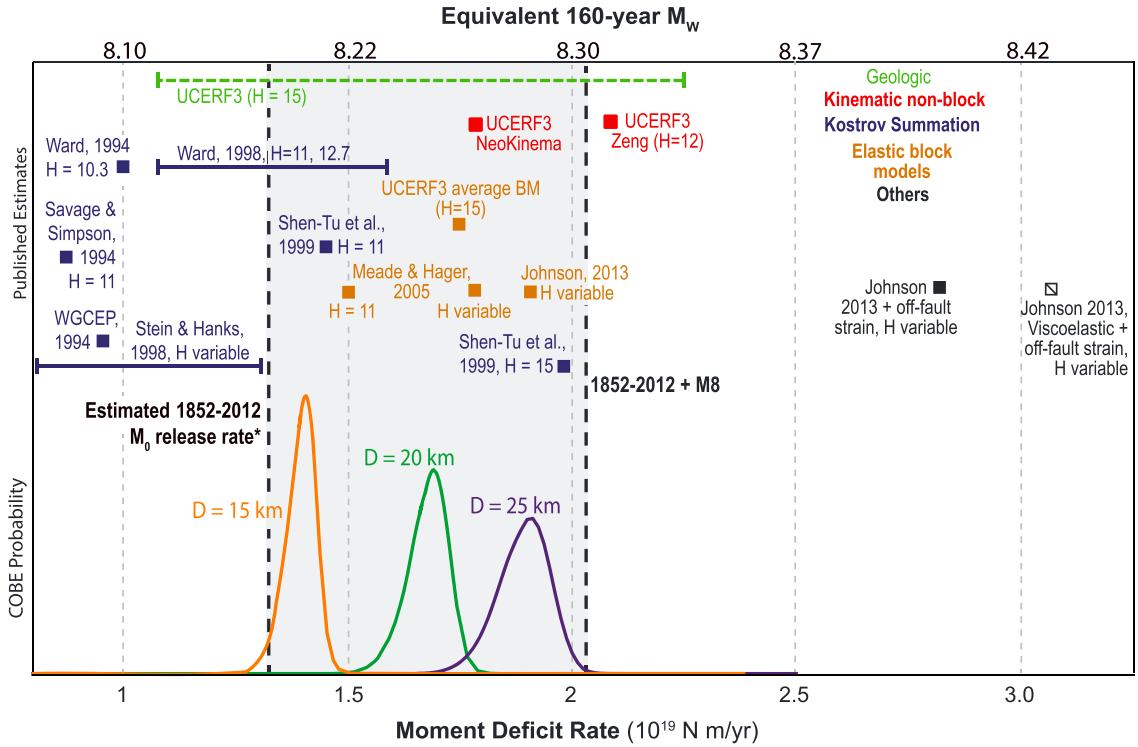

Figure 1. Estimates of the MDR for Southern California from previously published studies (upper half) and this study (lower half). Lower horizontal axis gives the MDR in Newton meters/year (N m/yr), and the upper horizontal axis is the equivalent 160-year earthquake magnitude for the entire region. Previous estimates are colored by model type, as shown in the legend, and assumed that faults are locked from the surface to a locking depth *H*. Estimates from the current study are colored by transition depth *D*, the depth to which slip deficit is permitted on block-bounding faults. The probability density functions (PDFs) are COBE estimates for the total Southern California fault system (Figure 3a) and do not include the off-fault MDR contribution, for example, as estimated by Johnson (2013). Left vertical black dashed line is the historic moment (see supporting information Figure S1); right is the historic plus an additional M_W 8. MDR = moment deficit rate; COBE = Constrained Optimization Bounding Estimator.

Other published studies used elastic block or plate-block models with specified locking depth *H*. In these models, blocks of crust are entirely enclosed by bounding faults and locked from the surface to depth *H*. Elastic block models assume an elastic half-space, while the plate-block model assumes an elastic crust overlying an inviscid half-space (Johnson, 2013). UCERF3 included five elastic block models that yielded an average moment accumulation rate of 1.73×10^{19} N m/yr (M_W 6.8), shown by an orange square in Figure 1. Meade and Hager (2005) used an elastic block model to obtain MDR estimates of 1.5×10^{19} (M_W 6.75, $H = 11$ km) and 1.78×10^{19} N m/yr (M_W 6.8, *H* variable). Johnson (2013) found 1.87×10^{19} N m/yr (M_W 6.81) for an elastic plate-block model. These are shown by the orange squares in Figure 1. These studies assumed that all faults were locked from the surface to some locking depth and solved for the long-term slip rates on each fault and in some cases for the locking depth.

Johnson (2013) estimated off-fault MDR using the Kostrov method on the strain that cannot be attributed to back slip on faults forming boundaries of rigid blocks. The total moment (on fault and off fault) is shown by the solid black square in Figure 1. The off-fault MDR estimate assumed a seismogenic depth of 11 km and is approximately 9×10^{18} N m/yr (M_W 6.6), about 50% of the on-fault MDR estimate (Johnson, 2013). Finally, Johnson (2013) used a viscoelastic cycle model to estimate MDR solving for locking depths and slip rates and found that this increases the MDR estimate even further (hatchured black square in Figure 1; this estimate also includes off-fault MDR).

All of the models in Johnson (2013) imply moment accumulation rates at the high end or higher than rates computed from UCERF3 geologic fault slip rates. All of the models shown except three of the Kostrov-based methods imply moment accumulation rates as high or higher than the historical moment release rate during the 160-year period from 1852 to 2012.

Note that by directly comparing geodetic estimates of the MDR in Southern California to the observed moment rate, we assume that it is possible to extrapolate from the time scale of the geodetic data (years to decades) to the time scales over which the seismic moment budget balances, which may be several centuries for the San Andreas Fault (SAF) or even longer for some of the low slip rate faults in the system (e.g., Rockwell et al., 2016). In addition, there are very different assumptions between the geologic and geodetic estimates shown in the plot and between Kostrov-type and fault-based methods. Although we refer to all of these models as for *Southern California*, there are slight differences in the exact areas considered in each study. More significantly, there are differences in the type of data used (geologic, geodetic, and plate motion estimates) and the quantity and quality of geodetic data (e.g., years versus decades of data for GNSS). While it is probably not possible to completely reconcile these differences, Figure 1 emphasizes the need to understand the source of these differences and whether or not they are significant given the uncertainties related to each type of data and model.

1.2. Estimating Uncertainty in the MDR

Maurer et al. (2017) consider a number of published and potential methods for estimating uncertainty in the MDR and showed that most can fail under predictable circumstances. To address this and other issues, Maurer et al. (2017) developed the Constrained Optimization Bounding Estimator (COBE) method for estimating a probability density function (PDF) for the total MDR on fault systems using geodetic data. The COBE method, described in section 2.3, is an optimization-based method that allows for bounds on slip rate, as informed by geologic studies, while directly modeling uncertainty in the MDR, ideal for earthquake hazard studies.

We apply the COBE method to estimate bounds on the MDR in Southern California, using the elastic plate-block model of Johnson (2013) and GNSS data available from the Southern California Earthquake Center Crustal Motion Map version 4 (CMM4) database. Geologic bounds on slip rate were used by Johnson (2013) to constrain the long-term steady state fault slip rates that are used in this study to bound the SDR. We compare our results to the studies shown in Figure 1 and confirm that, given the model, the estimated MDR in Southern California is at least as high or higher than the historical moment release rate since 1850. Bounds on MDR from COBE approximately include the range of estimates from previously published elastic block models but only explain a fraction of the range in MDR estimated using different types of forward models. Thus, modeling uncertainty (also known as epistemic uncertainty) dominates MDR uncertainty in Southern California.

2. Methods

2.1. Model Description

To model the long-term steady state deformation, we use an elastic plate-block model for the Earth's crust in Z (Huang et al., 2010; Johnson, 2013; Johnson & Fukuda, 2010). Blocks of crust overlay an inviscid half-space and are bounded by faults. Long-term steady state slip rates (i.e., in the absence of fault coupling) are assumed to the be the sum of four components: (1) long-term (rigid) block rotation about Euler poles: $\mathbf{V}_{\text{block}}$, (2) cancelation of fault normal discontinuities introduced by the block motion: $\mathbf{V}_{\text{cancel}}$, (3) forward slip on dipping faults: $\mathbf{V}_{\text{ds}}$, and (4) a spatially variable strain rate, parameterized by cubic polynomials within blocks: $\mathbf{V}_{\text{strain}}$. These terms make up the total steady state velocity

$$\mathbf{V}_{\text{ss}} = \mathbf{V}_{\text{block}} + \mathbf{V}_{\text{strain}} + \mathbf{V}_{\text{cancel}} + \mathbf{V}_{\text{ds}}. \tag{2}$$

$\mathbf{V}_{\text{ds}}$ is given by $|\delta\mathbf{V}|/\cos(\theta)$; $\delta\mathbf{V}$ is the (horizontal) velocity discontinuity vector across the fault and θ is the fault dip. As in Johnson (2013), we calculate $\mathbf{V}_{\text{strain}}$ for the Transverse Ranges and Mojave blocks, parameterized by cubic polynomials. $\mathbf{V}_{\text{cancel}}$ corrects for fault opening or interpenetration, $\mathbf{V}_{\text{strain}}$ models permanent inelastic strain inside blocks, and $\mathbf{V}_{\text{ds}}$ ensures that the horizontal velocity field normal to the fault trace is continuous across dipping faults (see Johnson, 2013, and Johnson & Fukuda, 2010, for more details regarding the calculation of the steady state velocities). Figure 2 illustrates the steady state velocity components for an example block without dipping faults.

Johnson (2013) estimated $\mathbf{V}_{\text{ss}}$ for the plate-block model constrained by geologic bounds on fault slip rates; further details of the forward model are given in that study. We subtract the estimated long-term rate from the observed velocity field, discretize the block-bounding faults, and solve for $\mathbf{V}_{\text{bs}}$ on the individual patches using the elastic half-space solutions of Okada (1985). We discretize the SAF, San Jacinto, and Garlock Fault into elements approximately 14 km long; for all other faults the length varies but averages around 30 km (see Figure 6). We must specify a transition depth D (discretization depth) for the model below in which there is no coupling and faults creep at the long-term slip rate; we present results for $D = 15, 20$, and 25 km. The

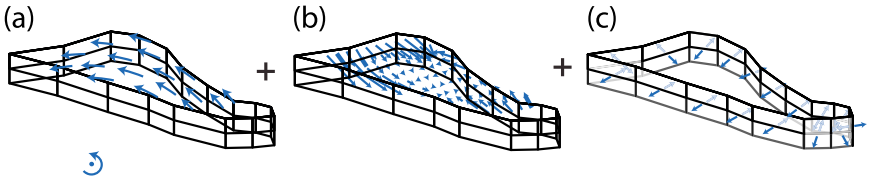

Figure 2. Illustration of how the steady state (long-term) velocity field $\mathbf{V}_{ss}$ is calculated: (a) $\mathbf{V}_{block}$, (b) $\mathbf{V}_{strain}$, and (c) $\mathbf{V}_{cancel}$. After Johnson and Fukuda (2010).

downdip width of the patch elements varies with *D*, because the same number of elements are used in all cases. The SAF, San Jacinto, and Garlock Fault are seven patches deep, while in all other faults we discretize four patches deep, including the dip-slip faults. The rest of the fault system includes the Eastern California Shear Zone, made up of the northern Sierra Range Front, Panamint Valley Fault, and Death Valley Fault, and the southern Mojave Desert faults. The Coast and Transverse Range faults include the Hosgri Fault and the Transverse Range Faults. The Peninsular Range Faults include the Elsinore Fault, Newport-Inglewood Fault, Palos Verdes Fault, San Clemente Fault, and southern SAF. As in Johnson (2013), we assume that all dipping faults have a dip of 45°.

The block model requires that we simplify the complex Southern California fault geometry into several fault-bounded blocks (Figure 3). The choice of block model faults is necessarily nonunique and is a source of epistemic uncertainty in our results (e.g., Evans, 2017). The predicted interseismic velocity field is then the sum of the steady state velocity field and the contribution resulting from the interseismic SDR or *back slip* rate on faults

$$\mathbf{V}_{pred} = \mathbf{V}_{ss} + \mathbf{V}_{bs}. \tag{3}$$

We assume that back slip is in the opposite direction of long-term slip. Johnson (2013) estimated dip-slip ($\dot{s}_{\infty}^{ds}$) and strike-slip $\dot{s}_{\infty}^{ss}$ components of $\mathbf{V}_{ss}$, subject to geologic constraints on slip rates. These estimates are applied as bounds on slip in this study. We solve for a single back slip rate in the rake direction implied by the dip-slip

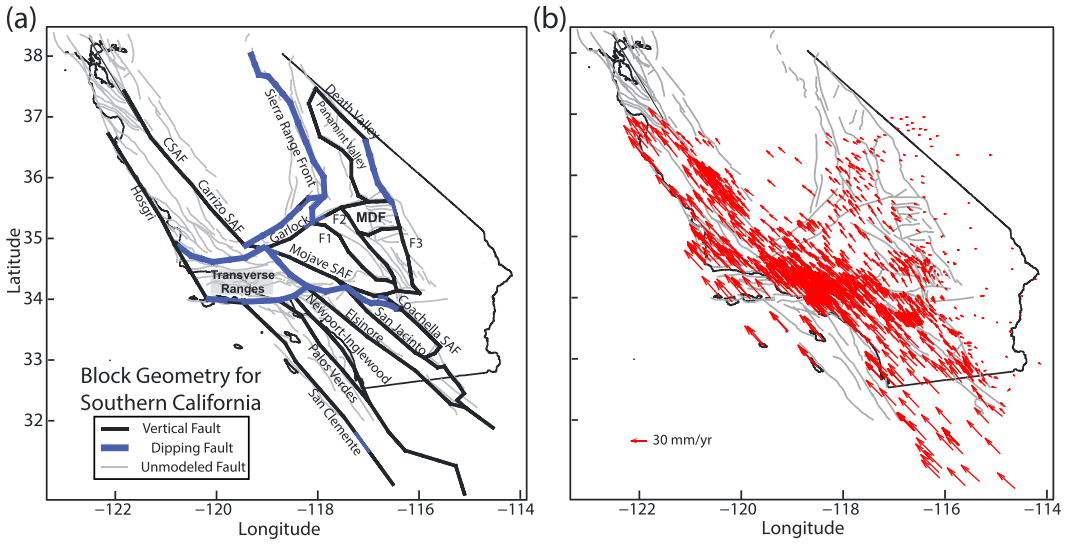

Figure 3. (a) Block boundary faults used in the inversion for MDR in Southern California, following Johnson (2013). Gray faults are from UCERF3. (b) GNSS velocities used in the inversion from the SCEC CMM4 (Shen et al., 2011); velocities are in stable North America reference frame. MDR = moment deficit rate; GNSS = Global Navigation Satellite Systems; UCERF3 = Unified California Earthquake Rupture Forecast; SCEC = Southern California Earthquake Center; CMM4 = Community Motion Map version 4; SAF = San Andreas Fault; CSAF = creeping segment of the SAF; MDF = southern Mojave Desert fault.

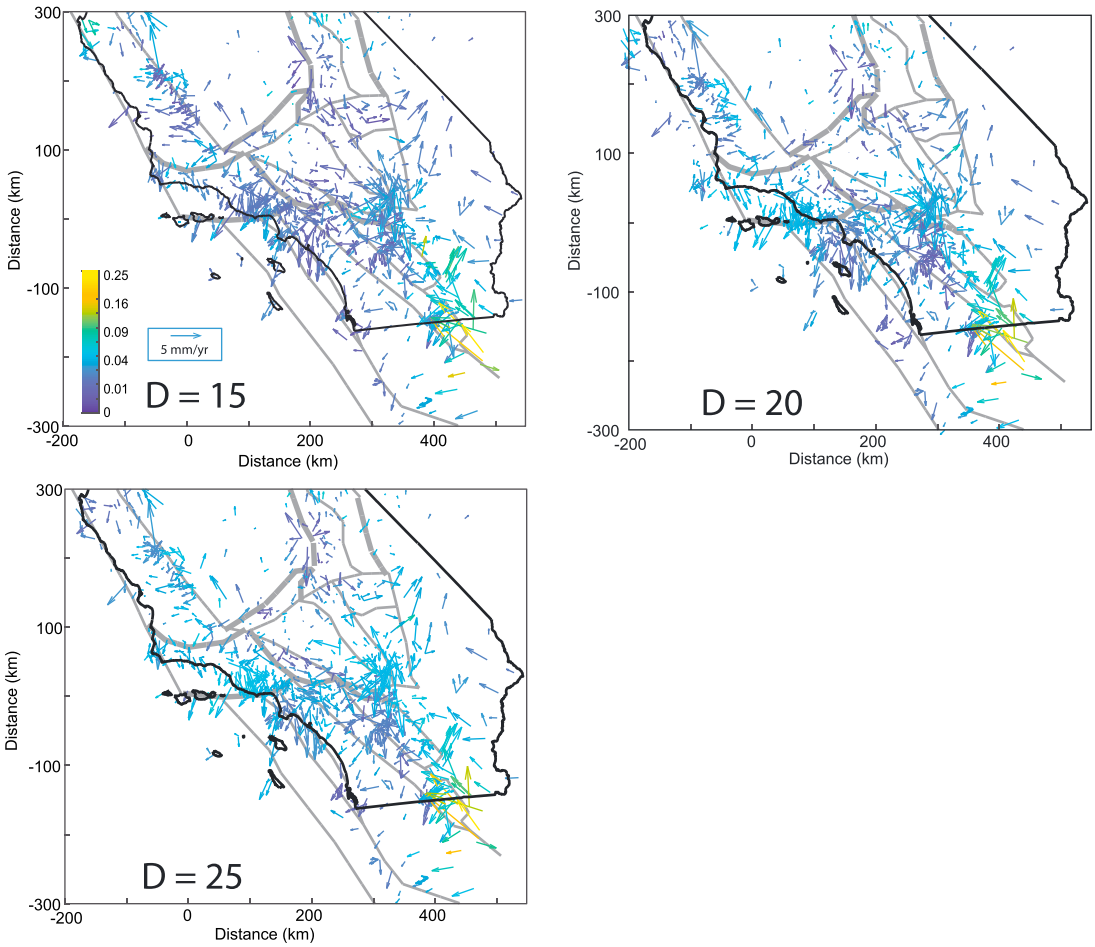

Figure 4. Global Navigation Satellite Systems residual vectors from the best fitting elastic plate-block model for each *D*, in millimeter/year. The color of the arrows indicates the magnitude of the difference in the residual velocities between the upper and lower 95% confidence bound models from the Constrained Optimization Bounding Estimator curve in millimeter/year (assuming a full covariance matrix).

and strike-slip components of $\mathbf{V}_{ss}$; the rake α on each fault patch is computed using

$$\alpha_i = \tan^{-1}\left(\frac{\dot{s}^{ds}_{\infty,i}}{\dot{s}^{ss}_{\infty,i}}\right), \tag{4}$$

where α_i is the rake on the ith patch and $\dot{s}^{ss}_{\infty,i}$ and $\dot{s}^{ds}_{\infty,i}$ are the strike-slip and dip-slip components of $\mathbf{V}_{ss}$ on the ith fault patch, respectively. To solve for the fixed-rake back slip rate, we combine the dip-slip and strike-slip Green's function matrices ($\mathbf{G}_{ds}$, $\mathbf{G}_{ss}$) obtained using Okada (1985) solutions to compute the overall Green's function for back slip $\mathbf{G}_{bs}$

$$\mathbf{G}_{bs} = \mathbf{G}_{ds}\sin(\alpha) + \mathbf{G}_{ss}\cos(\alpha). \tag{5}$$

2.2. Data and Uncertainties

We use a subset of the Southern California Earthquake Center CMM4 GNSS velocity field (Shen et al., 2011), shown in Figure 3b, to estimate back slip on crustal faults in Southern California. To do so, we compute and subtract $\mathbf{V}_{ss}$ from the observed geodetic surface velocities $\mathbf{V}_{obs}$ to obtain the residual velocity field

$$\mathbf{V}_r = \mathbf{V}_{obs} - \mathbf{V}_{ss}$$

We assume that the residual velocities $\mathbf{V}_r$ are due only to back slip on model faults plus noise.

The CMM4 field includes some stations that appear to have some contribution from transient deformation, in particular in the Mojave desert region due to the 1992 Landers and 1999 Hector Mine earthquakes. We

removed a subset of stations from the inversion and also subtracted a modeled velocity component due to deep postseismic creep on the *Camp Rock* fault segments of the southern Eastern California Shear Zone using buried dislocations 15–75 km deep, following Johnson (2013).

The CMM4 velocity field includes formal uncertainty estimates for each of the station velocities. These formal uncertainties are often quite small, owing the long observation times for some of the stations, much smaller than the prediction errors related to the block model. We impose a floor of 0.5 mm/year to avoid overfitting these stations.

As detailed in section 2.3, the COBE method depends directly on the data covariance matrix, which can be challenging to estimate; therefore, we use three different approaches to estimate it. Formal uncertainties are often increased or scaled in some manner (e.g., Fukuda & Johnson, 2008; Hsu et al., 2007; Maurer & Johnson, 2014; Segall et al., 2000) to account for additional sources of uncertainty, including spatial correlations between stations and model-dependent prediction errors resulting from an overly simplified Earth model. We follow this approach for the first covariance matrix, which uses the scaled formal errors (with the variance threshold and outliers removed, described above). The uncertainties are scaled such that the normalized variance of the residuals of the best fit model is approximately unity

$$\frac{(\mathbf{V_r}-\hat{\mathbf{V}}_\mathbf{r})^\intercal \Sigma^{-1}(\mathbf{V_r}-\hat{\mathbf{V}}_\mathbf{r})}{M} \approx 1, \tag{6}$$

where $\mathbf{\Sigma}$ is the covariance matrix, $\hat{\mathbf{V}}_r$ is the predicted data from the best fit SDR model, and we approximate the number of degrees of freedom with M, the number of data. The second covariance matrix also uses the scaled formal uncertainties, but in addition, we compute the empirical covariance between the east and north components of the GNSS data and add this constant value to the corresponding off-diagonal elements of the matrix. For the final covariance matrix, we use the best fit residuals $\mathbf{V}_r - \hat{\mathbf{V}}_r$ to estimate the average spatial covariance between all station pairs, for each pair of components (EE, NN, and EN). The full covariance matrix is composed of four $M \times M$ submatrices, fully populated by the scalar covariance for that block, plus the empirical component correlations (same as the tridiagonal matrix) and the formal uncertainties on the diagonal, with a minimum uncertainty threshold equal to the residual variance (Bruhat & Segall, 2017; Kato et al., 1998). The matrix is computed iteratively, initialized using the unweighted diagonal covariance. More details of the construction of these matrices are given in the supporting information.

2.3. The COBE for MDR

The COBE method, presented in Maurer et al. (2017), solves the following system:

$$\begin{aligned} p(\dot{M}_{\text{test}}|\mathbf{V}_r;\mathbf{\Sigma}) \quad &\equiv \max_{\dot{\mathbf{s}}} \text{lik}(\mathbf{V}_r|\dot{\mathbf{s}};\mathbf{\Sigma}) \\ \text{s.t.} \quad &\mathbf{a}^T\dot{\mathbf{s}} = \dot{M}_{\text{test}} \\ \text{and} \quad &\mathbf{0} \le \dot{\mathbf{s}} \le \dot{\mathbf{s}}_\infty \end{aligned} \tag{7}$$

or equivalently

$$\begin{aligned} p(\dot{M}_{\text{test}}|\mathbf{V}_r;\mathbf{\Sigma}) \equiv \max_{\dot{\mathbf{s}}} \text{lik}(\mathbf{V}_r|\dot{\mathbf{s}};\mathbf{\Sigma}) p_{\mathcal{U}}(\dot{\mathbf{s}};\mathbf{0},\dot{\mathbf{s}}_\infty) \\ \text{s.t. } \mathbf{a}^T\dot{\mathbf{s}} = \dot{M}_{\text{test}}, \end{aligned} \tag{8}$$

where $\dot{\mathbf{s}}$ is the vector of SDRs on each fault patch and $p_{\mathcal{U}}(\cdot;\mathbf{0},\dot{\mathbf{s}}_\infty)$ is the uniform PDF over SDR; that is, we assume that back slip is bounded between zero and the long-term rate $\dot{\mathbf{s}}_\infty$. Note that it is not possible to solve for the long-term slip rates with this method; instead, these must be supplied from geologic bounds on slip rate or, in our case, from geodetic estimates of steady state block motions constrained by geologic rates. The data likelihood function $\text{lik}(\mathbf{V}_r|\dot{\mathbf{s}};\mathbf{\Sigma})$ is Gaussian and parameterized by the covariance matrix $\mathbf{\Sigma}$ previously discussed. $\dot{M}_{\text{test}}$ is the moment deficit constraint. Systematically varying $\dot{M}_{\text{test}}$ from 0 (no deficit) to the maximum possible deficit, computing the probability at each point, and interpolating between the points gives the final PDF on MDR. We use the MATLAB function *lsqlin* to solve the constrained optimization problem in equation (8).

Note that equation (8) is not the Bayesian posterior probability distribution. A Bayesian probabilistic approach cannot be applied to estimate MDR as defined in equation (1) when bounds on slip are present due to mesh dependence in the solution. See Maurer et al. (2017) for more details.

Table 1
Summary of MDR Estimates for Southern California

D	Covariance type	95% MDR range ($\times 10^{19}$ N m/yr)	Annual M_W range	160-year M_W
15	Diagonal	1.37–1.43	6.72–6.74	8.19–8.21
15	Tridiagonal	1.32–1.46	6.71–6.74	8.18–8.21
15	Full	1.26–1.49	6.70–6.74	8.17–8.22
20	Diagonal	1.64–1.73	6.78–6.79	8.25–8.26
20	Tridiagonal	1.58–1.76	6.76–6.80	8.24–8.27
20	Full	1.50–1.81	6.75–6.80	8.22–8.27
25	Diagonal	1.84–1.95	6.81–6.83	8.28–8.30
25	Tridiagonal	1.77–1.99	6.80–6.83	8.27–8.30
25	Full	1.67–2.05	6.78–6.84	8.25–8.31

As discussed in Maurer et al. (2017), the COBE PDF is a conservative estimate of the uncertainty in MDR related to noisy data and the model null space. COBE does not model or include the prediction errors or *epistemic* uncertainty, for example, relating to the block model assumptions and geometry and assumed rheology. The COBE solution is for a given forward model, including fault geometry and crustal rheology. Note, however, that even with no data error (zero formal uncertainties) the COBE PDF need not have zero width. If some nontrivial part of the model space maps to zero in the data space (the definition of the model null space), then any model within that space will be given equal nonzero probability by the COBE estimator.

We present results for the full Southern California fault system in the next section obtained using the COBE method with the data and models described above. It is also possible to estimate joint PDFs on MDR for individual fault segments, as described in Maurer et al. (2017). We estimate PDFs on individual faults in Southern California and present the results below and in the supporting information.

3. Results

3.1. COBE Estimates for the Total Fault System

We estimated MDR for the full Southern California block model using the COBE method. Figure 1 shows PDFs for different transition depths, D, using the full covariance matrix, and Table 1 summarizes the results. Table 1 also gives results obtained using the diagonal and tridiagonal covariance matrices. Note that we obtain lower MDR estimates than other studies using comparable locking depths because slip deficit varies spatially on the faults (see supporting information Figures S1–S3), rather than being fixed with depth.

The bounds on MDR obtained using the full covariance matrix and a single model are much narrower (by about a factor of 8) than the range of estimates considering different types of forward models (such as Kostrov summation or viscoelastic models) and potential off-fault MDR. This shows that the uncertainty in MDR stemming from the data uncertainty and lack of resolution is small relative to the uncertainty implied by different model choices (i.e., block model vs. kinematic nonblock vs. viscoelastic, etc). As discussed below, whether or not a block model in which the crust can only deform elastically is even appropriate for Southern California is an important question and a topic for further research.

Figure 4 shows the GNSS residuals for the best fitting SDR model for each depth D. For most stations, there is little difference between end-member models compared to the absolute size of the residuals. Systematic trends in the residuals, likely indicating errors in the forward model, exist near the southern SAF, the Tranverse Ranges, and eastern Mojave desert region. Much of these are due to the simplified block geometry; in particular, we have accounted for dipping faults in the Transverse Ranges in a very simplified way. There is also unmodeled extension occurring near the southern SAF. It is clear from Figure 4 that the residuals can change quite drastically across block boundaries.

Figure 5 shows the absolute strike-slip SDR models from the MLE for each D, and supporting information Figures S1–S3 show the coupling ratios for the 95% end-member models and the MLE model, for each depth D. Note that these slip distributions are not realistic images of the spatial distribution of slip deficit in Southern California. Differences in coupling between end-member models are seen especially on the off-shore faults (San Clemente, Palos Verde, and Hosgri) and the faults in northeastern California (Sierra Range Front,

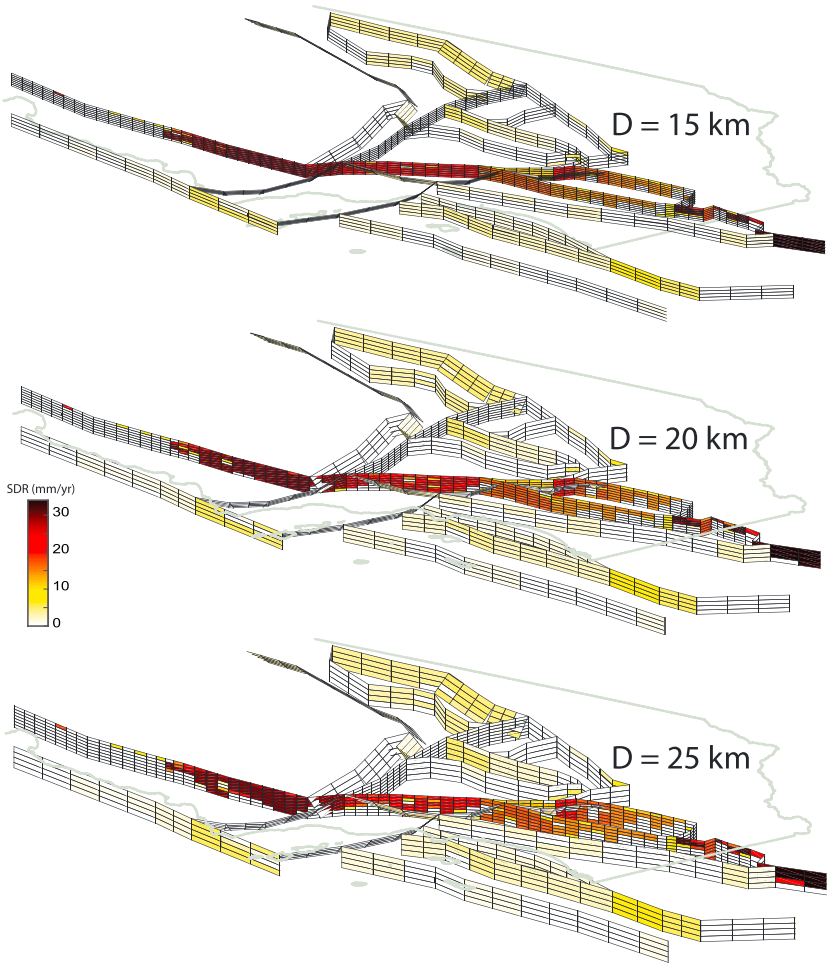

Figure 5. Strike-slip component of the best fitting SDR for each transition depth *D*. SDR = slip deficit rate.

Panamint Valley, and Death Valley). In general, the San Andreas and San Jacinto Faults are well constrained by the high data density, including stations relatively far from the faults; as a result there are very small differences between end-member models. Comparing the SDR on the SAF to the along-strike variable locking depth of Johnson (2013) also shows very good agreement, albeit with the finer resolution of the current model geometry.

3.2. COBE Estimates for Individual Faults

We estimate the MDR on individual fault segments and subregions of Southern California. This can be done by constraining MDR on a selected individual fault while allowing the MDR on all other faults to be unconstrained; alternatively, several segments can be simultaneously constrained in a multidimensional grid search approach to obtain fault-wise correlations (Maurer et al., 2017). Figure 6 shows the results for a transition depth of 20 km. The creeping segment of the SAF (CSAF), the Hosgri Fault, Garlock Fault, and the southern half of the Eastern California Shear Zone all have MDRs less than 10^{18} N m/yr. The mode for the CSAF indicates a very low MDR, with the long positively skewed tail indicating that the data can be fit allowing some moment accumulation at depth. In contrast, the SAF-Carrizo plain, SAF-Mojave Desert, and San Jacinto Fault segments all have high deficit rates, corresponding to 160-year earthquakes of $M_W \approx 7.6–7.8$. Faults on the outskirts of the network have poorly resolved MDR, including the off-shore faults (collected together into the "Peninsular Range faults") and the northern Eastern California Shear Zone faults that extend into the Basin and Range Province in Nevada. MDR on these two systems can vary by factors of 2–3 and still fit the data. Supporting information Figure S4 shows segment results for a transition depth of 25 km. Details on these segments, as well as the individual faults that comprise the larger groups, can be found in supporting information Tables S1 (D = 20 km) and S2 (D = 25 km).

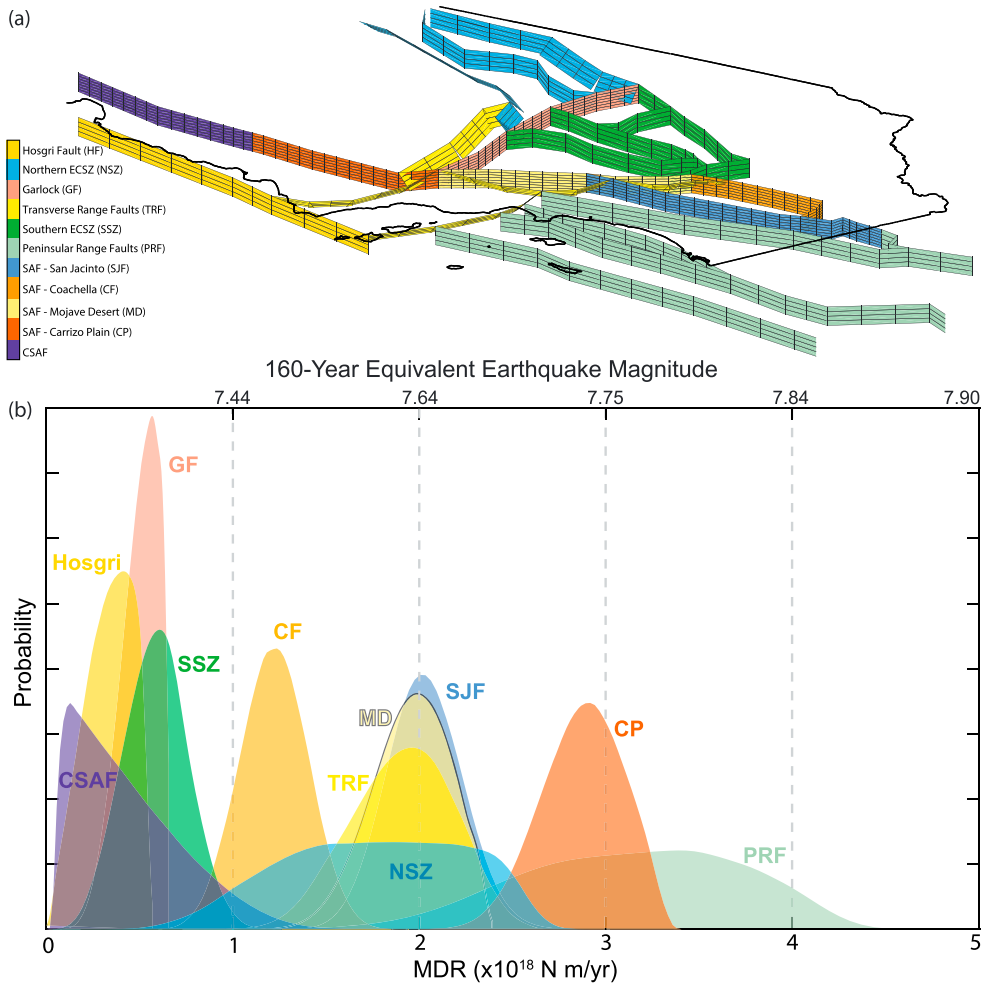

Figure 6. (a) Division of the block model into individual segments and subregions. (b) COBE PDFs on MDR for the segments shown in (a), obtained using the full covariance matrix. Axes are the same as in Figure 1. COBE = Constrained Optimization Bounding Estimator; MDR = moment deficit rate; SAF = San Andreas Fault; CSAF = creeping segment of the SAF.

It is of interest to know how strongly correlated the MDR estimates are for subparallel fault strands such as the San Jacinto, Elsinore, and SAF-Coachella. We estimated correlations for several sets of faults using the multidimensional COBE method as described in Maurer et al. (2017), but in general, we found that correlations were very small to nonexistent. To demonstrate this, note that total MDR is the sum of the MDRs on each segment. For uncorrelated segment estimates, the variance of the MDR estimate for the full system should approximately match the sum of the variances for the segments. We approximated the variance on MDR for each segment shown in Figure 6 by dividing the 95% confidence bound (given in tables in the supporting information) by four and squaring and compared the sum for all segments to the total system. The standard deviation of the sum is 9.0×10^{17} N m/yr, very similar to the total of 7.7×10^{17} N m/yr for $D = 20$ km, indicating uncorrelated PDFs. The lack of significant correlation is likely due to the kinematic constraints of the block model, and it suggests that estimates of MDR on individual fault segments for the block model are largely independent.

4. Discussion

4.1. Model Uncertainty in COBE-Based MDR Estimates

Our estimate of bounds on MDR using the COBE method provides first-order constraints on the accumulating moment deficit in Southern California. However, it is important to clarify that COBE provides conservative bounds on MDR given one choice of a forward model and one choice for the covariance matrix Σ; the

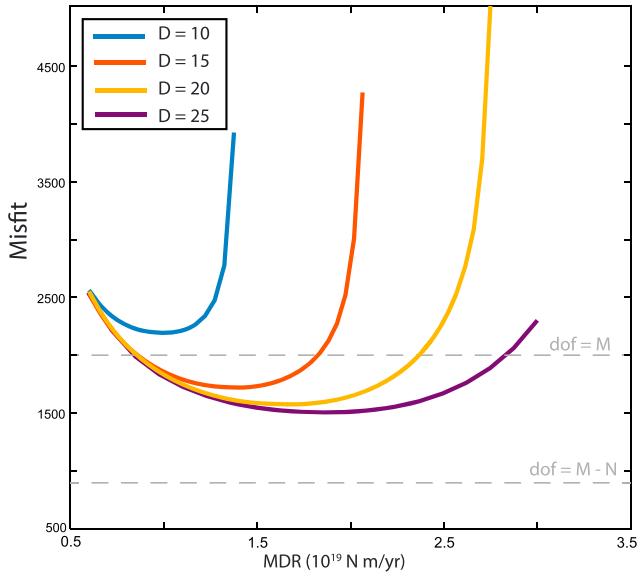

Figure 7. Misfit versus moment deficit rate computed using the block model for Southern California shown in Figure 1a in the main text, with four different discretization depths *D*: 10, 15, 20, and 25 km. The two horizontal dashed lines correspond to different χ^2 cutoffs, assuming lower (*M*-*N*) or higher (*M*) values for degrees of freedom, where *M* is the number of data and *N* is the number of fault patches.

epistemic uncertainty related to the choice of a particular forward model, with all inherent simplifications and assumptions, is a separate source of uncertainty that is clear from Figure 1. Block model assumptions, geometry, and crustal rheology among others are not accounted for with this method, unless the associated uncertainty can be included in the covariance matrix (e.g., Diner & Özgün Konca, 2017; Duputel et al., 2014). Even assuming the elastic plate-block model, there are several important choices that must be made regarding the model, all of which have their own associated uncertainties that are not measured in our study. These include the transition depth, *D*, the choice of block geometry, the shear modulus, *G*, and the long-term slip rate $\mathbf{V}_{ss}$ (see equation (7)). Regarding slip rates, Johnson (2013) showed that uncertainties in the geodetic estimates of $\mathbf{V}_{ss}$ conditioned on our choice of block model are relatively small. We use a constant value of 30 GPa for shear modulus for all of our moment estimates; reducing this by a third would match the curve for $D = 20$ km to the historical moment rate.

The *transition depth*, *D*, refers to the depth of discretization in the model, and therefore the maximum depth of slip deficit, which has a strong impact on both the overall uncertainty of the results and the actual MDR estimate. This parameter is different from the locking depth estimated in Johnson (2013) and other block models. The transition depth, *D*, cannot be uniquely determined using only surface deformation data; deeper transition depths will always fit the data at least as well or better than shallower depths because slip deficit deep on the fault has minimal impact on surface data but may significantly contribute to the overall MDR. This is demonstrated in Figure 7, which shows four misfit-versus-MDR curves for four different transition depths ranging from 10 to 25 km, leaving all other factors the same (number of fault patches, etc). The examples shown use the tridiagonal covariance matrix, with weights computed assuming $D = 20$ km. For a given covariance estimate, deeper transition depths fit better, presumably because greater *D* allows spatially variable slip deficit at depth to fit small variations in the data.

From Figure 5, the depth extent of SDR along the San Andreas is well constrained due to the abundance of data. In other regions without the far-field observations required to constrain the total moment, additional sources of data beyond geodesy, such as the depth extent of seismicity and seismic slip in large earthquakes, will need to be considered to determine what transition depths are realistic for Southern California.

The choice of block boundaries is an obvious potential source of systematic misfits and epistemic uncertainty. Southern California is a geologically complex region, with active folding and potentially many small faults accommodating diffuse deformation, especially in the Transverse Ranges and the Mojave block sections near the Big Bend in the SAF (Johnson, 2013; Ward, 1998). Simplifying these to a few large blocks that behave elastically is a major simplification that could potentially introduce a bias toward larger moment. Indeed, it is an open question whether or not elastic block or plate-block models, which allow only elastic deformation in the crust, are appropriate models for Southern California at all.

4.2. Discrepancy Between Observed and Estimated Moment in Southern California

Our estimates of the MDR are consistent with other studies that show that the current moment accumulation rate in Southern California is greater than the average annual seismic moment rate since 1850. As noted in section 1.1, a small fraction of the discrepancy between prior estimates shown in Figure 1 could be due to differences in the study area or more importantly differences in the available data. However, it is important to note that the SAF alone, based on our estimates, contributes about 50% of the total deficit for $D = 20$ km (see the tables in the supporting information), and an even larger fraction for smaller transition depths. The large differences in estimated MDR are more likely due to differences in the data and model than to the slight differences in the formal study area. The estimated historic moment is right at the lower bound of allowed moment using the smallest transition depth (15 km) with the COBE method, without accounting for off-fault MDR. There are at least four possible reasons that could account for some or all of the discrepancy between observed and estimated moment:

1. MDR estimates are balanced in part by moment released aseismically, including as postseismic transient deformation. Because only coseismic moment is included in the historic moment estimate, it is a lower bound on the total moment since 1850. In particular, transient aseismic slip following earthquakes (afterslip) may account for a significant fraction of the total moment release on some faults. This has been documented at Parkfield for both the 1966 and 2004 earthquakes (e.g., Lienkaemper & McFarland, 2017; Smith & Wyss, 1968), although the amount of afterslip at Parkfield may be extreme because of its proximity to the nearby creeping section. Other earthquakes on strike-slip faults have postseismic moment of 15–30% of the coseismic (e.g., Floyd et al., 2016; Reilinger et al., 2000). Assuming that transient aseismic slip on average adds an additional 20% to the total moment brings the historical estimate up to approximately 1.6×10^{19} N m/yr, close to the elastic plate-block results obtained in this study for $D = 20$ km.
2. It may be that there will be future earthquakes that *catch up* the observed moment to the estimated (e.g., Ward, 1998). The existing historic earthquake record in Southern California may simply be too short to obtain an accurate estimate of the long-term moment rate. If this is true, it could potentially indicate that there is currently a deficit of major earthquakes in Southern California relative to the long-term rate. Moreover, there is evidence of long-term variations in the earthquake recurrence rates (Rockwell et al., 2016).
3. There could be long-term changes in surface deformation rates that would lead to overall lower moment accumulation in the last 150 years. A problem with this explanation is that one known mechanism for causing such time-dependent deformation—namely, viscoelastic relaxation in the lower crust—predicts the opposite sign, according to one analysis (Johnson, 2013), as shown in Figure 1. (This result does depend on what point we are in the earthquake cycle; the higher MDR stems from assuming that the current time is late in the cycle, so observed strain rates are lower than average.) Other time-dependent mechanism would have to be active to reduce the MDR. Some studies have suggested that major faults in Southern California may have experienced changes in slip rate over time scales spanning several earthquake cycles (e.g., Bennett et al., 2004; Onderdonk et al., 2015; Sharp, 1981). Proposed mechanisms for such changes include earthquake clustering or unusually large slip during several events (Onderdonk et al., 2015) or changes in the slip partitioning between faults over time (Bennett et al., 2004; Sharp, 1981).
4. A final possibility is that there may be some fraction of the MDR that is taken up in permanent inelastic deformation that is never recovered seismically. Related to this is the fact that any fully elastic model cannot capture all of the mechanics of deformation in Southern California, such as folding, pressure solution, and plastic yielding including permanent deformation associated with nonplanar fault geometry. This would reduce the total moment available to drive earthquakes and thus reduce the discrepancy. None of the models shown in Figure 1 fully address these issues, and only one considers possible time dependence due to viscoelastic effects. It is clear that more work is needed to develop realistic crustal models that reflect all of the processes that occur on time scales of the largest earthquakes.

4.3. Off-Fault Deformation in Southern California

Related to the last point, there must be some internal block deformation that is not attributable to back slip on regional faults; some deformation must occur within the blocks due to smaller faults that are omitted from the model. Johnson (2013) used the nonrigid body terms in equation (2) to compute an estimate of *off-fault* moment deficit: $\mathbf{V}_{ds} + \mathbf{V}_{cancel} + \mathbf{V}_{strain}$, by isolating this component of the velocity field, computing surface strain rates, and integrating to get moment rate (Savage & Simpson, 1997). The total moment rate for the region was $\sim 9 \times 10^{18}$ N m/yr for Southern California, almost 50% of the estimated on-fault MDR for the elastic plate-block model (see Table 2 in Johnson, 2013).

This number is included in both of the models shown by the black squares in Figure 1. This off-fault MDR significantly increases the discrepancy with the observed seismic moment. However, folding and uplift in areas such as the Transverse Ranges and San Gabriel mountains clearly indicates that some amount of permanent inelastic deformation occurs in Southern California. Geodetic measurements alone cannot distinguish between elastic and inelastic strain, and due to uncertainty in the average historic moment rate one cannot simply compare historic seismicity to the geodetic estimate. Holocene fault slip rates provide critical information, but it is clear in Figure 1 that the uncertainty from considering only geologic bounds on MDR is larger than the geodetic bounds. Due to these issues, it is unknown what fraction of the estimated off-fault MDR is permanent inelastic strain or recoverable elastic strain across smaller faults not included in the model. We leave it to future work to investigate in more detail how and where this off-fault moment deficit fits into the overall moment budget for Southern California.

5. Conclusions

1. We have applied the COBE method to estimate the MDR in Southern California using the CMM4 GNSS database and an elastic plate-block model and find an MDR up to 56% greater than the observed seismic moment release since 1850, depending on assumed transition depth D. For $D = 20$ km, the estimated MDR is enough such that, extrapolated to 1850, enough moment should have accumulated to exceed the moment released in all historical events during that period, including the 1857 Fort Tejon earthquake, even ignoring the potential of off-fault moment deficit.
2. The uncertainty in MDR stemming from the data and imperfect model resolution is small relative to the uncertainty stemming from choice of deformation model for Southern California. There is much room for improvement in the quantification of prediction errors for a given model and in general for models that account for inelastic deformation of the crust.
3. There is a discrepancy between the geodetically estimated MDR and historic seismicity since 1850, particularly for models that include an estimate of the off-fault MDR. There are a number of possible reasons for the discrepancy, including afterslip, inelastic deformation, and future large earthquakes.
4. MDR on individual fault segments varies across the region. Uncertainties correlate inversely with data density the presence of far-field stations: lowest for the SAF and highest for the off-shore faults and Basin and Range province. MDR estimates on individual faults are not highly correlated with one another due to constraints implicit in elastic block models. Segment-wise estimates of MDR give further detailed information on where MDRs are highest and provide clues as to where more data would be most beneficial for constraining MDR.
5. We have shown by example in this study that the MDR can be robustly estimated using the COBE method. This direct estimate of the MDR and its uncertainty effectively bypasses the inherent ambiguity of using SDR models alone for seismic hazard studies. Instead, direct measurement of bounds on MDR can inform seismic hazard studies on both fault and fault system scales, and coupled with other data can provide valuable constraints on seismic hazard from geodesy.

Acknowledgments
This work was supported in part by Proposal 14058 from the Southern California Earthquake Center. SCEC is funded by the NSF Cooperative Agreement EAR-0529922 and the USGS Cooperative Agreement 07HQAG0008. This work was done as a private venture and not in the author's (J. M.) current capacity as an employee of the Jet Propulsion Laboratory, California Institute of Technology. GNSS data used in this study is available at http://scec.ess.ucla.edu/~zshen/cmm4/cmm4.html, last accessed Friday, 9 March 2018. Seismicity data to estimate the moment release for 1852–2012 was obtained from https://pubs.usgs.gov/of/2013/1165/, last accessed Friday, 9 March 2018. The block model used in this study is from Johnson (2013). We thank the Associate Editor and Jean-Philippe Avouac and an anonymous reviewer for their helpful comments which substantially improved the manuscript.

References

Bennett, R. A., Friedrich, A. M., & Furlong, K. P. (2004). Codependent histories of the San Andreas and San Jacinto fault zones from inversion of fault displacement rates. *Geology*, *32*(11), 961–964.

Bird, P. (2009). Long-term fault slip rates, distributed deformation rates, and forecast of seismicity in the western United States from joint fitting of community geologic, geodetic, and stress direction data sets. *Journal of Geophysical Research*, *114*, B11403. https://doi.org/10.1029/2009JB006317

Bruhat, L., & Segall, P. (2017). Deformation rates in northern Cascadia consistent with slow updip propagation of deep interseismic creep. *Geophysical Journal International*, *211*(1), 427–449. https://doi.org/10.1093/gji/ggx317

Diner, Ç., & Özgün Konca, A. (2017). Moment tensor for seismic sources on a bimaterial interface: A hyperfunction approach. *Bulletin of the Seismological Society of America*, *107*, 652–659. https://doi.org/10.1785/0120160044

Duputel, Z., Agram, P. S., Simons, M., Minson, S. E., & Beck, J. L. (2014). Accounting for prediction uncertainty when inferring subsurface fault slip. *Geophysical Journal International*, *197*, 464–482. https://doi.org/10.1093/gji/ggt517

Evans, E. L. (2017). A comprehensive analysis of geodetic slip-rate estimates and uncertainties in California. *Bulletin of the Seismological Society of America*, *108*, 1–18. https://doi.org/10.1785/0120170159

Feigl, K. L., Agnew, D. C., Bock, Y., Dong, D., Donnellan, A., Hager, B. H., et al. (1993). Space geodetic measurement of crustal deformation in central and southern California, 1984–1992. *Journal of Geophysical Research*, *98*(B12), 21,677–21,712.

Field, E. H. E., Arrowsmith, R. J., Biasi, G. P. G., Bird, P., Dawson, T. E. T., Felzer, K. R., et al. (2014). Michael uniform California earthquake rupture forecast, version 3 (UCERF3): The time-independent model. *Bulletin of the Seismological Society of America*, *104*(3), 1122–1180.

Floyd, M. A., Walters, R., Elliott, J., Funning, G., Svarc, J., Murray, J., et al. (2016). Spatial variations in fault friction related to lithology from rupture and afterslip of the 2014 South Napa, California, earthquake. *Geophysical Research Letters*, *43*, 6808–6816. https://doi.org/10.1002/2016GL069428

Fukuda, J. J., & Johnson, K. M. (2008). A fully Bayesian inversion for spatial distribution of fault slip with objective smoothing. *Bulletin of the Seismological Society of America*, *98*(3), 1128–1146. https://doi.org/10.1785/0120070194

Hsu, Y.-J., Segall, P., Yu, S.-B., Kuo, L.-C., & Williams, C. A. (2007). Temporal and spatial variations of post-seismic deformation following the 1999 Chi-Chi, Taiwan earthquake. *Geophysical Journal International*, *169*(2), 367–379. https://doi.org/10.1111/j.1365-246$\times$.2006.03310.x

Huang, W.-J., Johnson, K. M., Fukuda, J., & Yu, S.-B. (2010). Insights into active tectonics of eastern Taiwan from analyses of geodetic and geologic data. *Journal of Geophysical Research*, *115*, B03413. https://doi.org/10.1029/2008JB006208

Johnson, K. M. (2013). Slip rates and off-fault deformation in Southern California inferred from GPS data and models. *Journal of Geophysical Research: Solid Earth*, *118*, 5643–5664. https://doi.org/10.1002/jgrb.50365

Johnson, K. M., & Fukuda, J. (2010). New methods for estimating the spatial distribution of locked asperities and stress-driven interseismic creep on faults with application to the San Francisco Bay Area, California. *Journal of Geophysical Research*, *115*, B12408. https://doi.org/10.1029/2010JB007703

Kato, T., El-Fiky, G. S., Oware, E. N., & Miyazaki, S. (1998). Crustal strains in the Japanese islands as deduced from dense GPS array. *Geophysical Research Letters*, *25*(18), 3445–3448. https://doi.org/10.1029/98GL02693

Lienkaemper, J. J., & McFarland, F. S. (2017). Long-term Afterslip of the 2004 M 6.0 Parkfield, California, Earthquake—Implications for forecasting amount and duration of afterslip on other major creeping faults. *Bulletin of the Seismological Society of America*, *107*(3), 1082–1093.

Maurer, J., & Johnson, K. (2014). Fault coupling and potential for earthquakes on the creeping section of the central San Andreas Fault. *Journal of Geophysical Research: Solid Earth*, *119*, 4414–4428. https://doi.org/10.1002/2013JB010741

Maurer, J., Segall, P., & Bradley, A. M. (2017). Bounding the moment deficit rate on crustal faults using geodetic data: Methods. *Journal of Geophysical Research: Solid Earth*, *122*, 6811–6835. https://doi.org/10.1002/2017JB014300

Meade, B. J., & Hager, B. H. (2005). Spatial localization of moment deficits in southern California. *Journal of Geophysical Research*, *110*, B04402. https://doi.org/10.1029/2004JB003331

Okada, Y. (1985). Surface deformation due to shear and tensile faults in a half-space. *Bulletin of the Seismological Society of America*, *75*(4), 1135–1154.

Onderdonk, N. W., McGill, S. F., & Rockwell, T. K. (2015). Short-term variations in slip rate and size of prehistoric earthquakes during the past 2000 years on the northern San Jacinto fault zone, a major plate-boundary structure in southern California. *Lithosphere*, *7*(3), 211–234.

Reilinger, R. E., Ergintav, S., Bürgmann, R., McClusky, S., Lenk, O., Barka, A., et al. (2000). Coseismic and postseismic fault slip for the 17 August 1999, $M = 7.5$, Izmit, Turkey earthquake. *Science*, *289*(5484), 1519–1524.

Rockwell, T., Scharer, K., & Dawson, T. (2016). Earthquake geology and paleoseismology of major strands of the San Andreas Fault system. In R. Anderson & H. Ferriz (Eds.), *Applied geology in California* (pp. 721–756). Belmont CA: Star Publishing Co. Inc.

Savage, J. C., & Simpson, R. W. (1997). Surface strain accumulation and the seismic moment tensor. *Bulletin of the Seismological Society of America*, *87*(5), 1345–1353.

Segall, P., Bürgmann, R., & Matthews, M. (2000). Time-dependent triggered afterslip following the 1989 Loma Prieta earthquake. *Journal of Geophysical Research*, *105*(B3), 5615–5634. https://doi.org/10.1029/1999JB900352

Sharp, R. V. (1981). Variable rates of Late Quaternary strike slip on the San Jacinto Fault Zone, southern California. *Journal of Geophysical Research*, *86*(B3), 1754–1762. https://doi.org/10.1029/JB086iB03p01754

Shen, Z.-K. K., King, R. W., Agnew, D. C., Wang, M., Herring, T. A., Dong, D., & Fang, P. (2011). A unified analysis of crustal motion in Southern California, 1970–2004: The SCEC crustal motion map. *Journal of Geophysical Research*, *116*, B11402. https://doi.org/10.1029/2011JB008549

Shen-Tu, B., Holt, W. E., & Haines, A. J. (1999). Deformation kinematics in the western United States determined from Quaternary fault slip rates and recent geodetic data. *Journal of Geophysical Research*, *104*(B12), 28,927–28,955.

Smith, S. W., & Wyss, M. (1968). Displacement on the San Andreas fault subsequent to the 1966 Parkfield earthquake. *Bulletin of the Seismological Society of America*, *58*(6), 1955–1973.

Stein, R. S., & Hanks, T. C. (1998). M $\geq$ 6 earthquakes in southern California during the twentieth century: No evidence for a seismicity or moment deficit. *Bulletin of the Seismological Society of America*, *88*(3), 635–652.

Ward, S. N. (1994). A multidisciplinary approach to seismic hazard in southern California. *Bulletin of the Seismological Society of America*, *84*(5), 1293–1309. https://doi.org/10.1016/0148-9062(95)96940-D

Ward, S. N. (1998). On the consistency of earthquake moment rates, geological fault data, and space geodetic strain: The United States. *Geophysical Journal International*, *134*(1), 172–186.

Zeng, Y., & Shen, Z.-K. (2014). Fault network modeling of crustal deformation in California constrained using GPS and geologic observations. *Tectonophysics*, *612*, 1–17. https://doi.org/10.1016/j.tecto.2013.11.030